Optimal Path-Planning of Nonholonomic Terrain Robots for Dynamic Obstacle Avoidance Using Single-Time Velocity Estimator and Reinforcement Learning Approach

Taghavifar, H., Xu, B., Taghavifar, L. & Qin, Y.

Optimal Path-Planning of Nonholonomic Terrain Robots for Dynamic Obstacle Avoidance Using Single-Time Velocity Estimator and Reinforcement Learning Approach

HAMID TAGHAVIFAR [1], (Member, IEEE), **BIN XU** [2,3], **LEYLA TAGHAVIFAR** [4],
AND YECHEN QIN [2], (Member, IEEE)
[1] School of Mechanical, Aerospace and Automotive Engineering, Coventry University, Coventry CV1 2JH, U.K.
[2] School of Mechanical Engineering, Beijing Institute of Technology, Beijing 100081, China
[3] Chongqing Innovation Center, Beijing Institute of Technology, Chongqing 401147, China
[4] Department of Electrical and Electronics Engineering, IAU, Tehran 1477893855, Iran

Corresponding author: Bin Xu (bitxubin@bit.edu.cn)

ABSTRACT A single-time velocity estimator-based reinforcement learning (RL) algorithm, integrated with a chaotic metaheuristic optimization technique is proposed in this article for the optimal path-planning of the nonholonomic robots considering a moving/stationary obstacle avoidance strategy. The additional contribution of the present study is by employing the Terramechanics principles to incorporate the effects of wheel sinkage into the deformable terrain on the dynamics of the robot aiming to find the optimal compensating force/torque magnitude to sustain a robust and smooth motion. The designed systematic control-oriented system incorporates a cost function of weighted components associated with the target-tracking and the obstacle avoidance. The designed velocity estimator contributes to the finite-state Markov decision process (MDP) in order to train the transition probabilities of the problem objectives. Based on the obtained results, the optimal solution for the Q-learning in terms of the adjusting factor for the minimized tracking error and obstacle collision risk propagation profiles is found at 0.22. The results further confirm the promising capacity of the proposed optimization-based RL algorithm for the collision avoidance control of the nonholonomic robots on deformable terrains.

INDEX TERMS Mechatronics, terramechanics, path-planning, artificial intelligence.

I. INTRODUCTION

Autonomous mobile robots are massively employed in the hazardous environments such as military operations, space explorations, and mining industries to eliminate the risk that the human labour is being exposed [1], [2]. Likewise, wheeled robots are also utilized in the farmlands during various agricultural operations such as weed detection/elimination for the precision farming and optimized productivity [3], [4]. Thus, mobile robots should hold the ability of route finding, high manoeuvrability, and optimal self-positioning in the plane of motion under different operating conditions such as the road condition variability which drastically affects the dynamic response of the moving vehicles [5]–[7]. Obstacle avoidance

feature is also regarded as one of the substantial consideration related to the functional design of task-assigned automatic wheeled robots [8].

The presence of matched and mismatched uncertainties such as moving obstacles and robots, cluttered environment and unstable operating conditions aggravate the optimal design of autonomous robots [1]. Additionally, provision of automated robots with the logic to find the optimal path in terms of the nearest and safest route to take is still considered as a challenging task [9], [10]. Therefore, intelligent vehicle navigation systems based on self-organizing/self-training aptitude have gained a growing attention in the field of autonomous wheeled robots.

Local obstacle avoidance techniques are employed online in the absence of global information, typically via popular methods such as artificial potential fields (APFs) [11],

The associate editor coordinating the review of this manuscript and approving it for publication was Chao Shen.

vector field histograms (VFH) [12], and the dynamic window approach (DWA) [13], which extends local avoidance approaches on account of kinematics constraints. Literature is abundant with various strategies proposed to address the problem of obstacle avoidance of automated robots [14]–[23]. In [14], a generic 2-wheeled automated robot with obstacle detection capacity was developed to deal with the nonholonomic constraints based on model predictive approach. The advantage of predictive model based techniques is the improved robot steerability in the time domain only if the reference model holds the capacity to satisfactorily predict the robot dynamic response. Biological-inspired control methods such as neurodynamics model hybridized with a backstepping technique has also shown effectiveness for the real-time path planning of non-holomic robots [15], [16]. In addition to the Lyapunov-based adaptive control paradigms, the online minimum-energy control strategies have shown a remarkable application for the path planning goals related to the wheeled omnidirectional robots as well [17]–[19].

Reinforcement learning (RL) is suggestive of a high-precision and hugely reliable method to achieve a range of pattern-recognition, modelling and control objectives within the complex domains that has found substantial application in the field of robotics [20]–[22]. For instance, a research was carried out to enable the robot for the mobility on an uncertain environment by inclusion of stationary and dynamic obstacles based on the integrated Q-learning and a neural network planner [23]. The developed strategy exhibited a proper performance in navigation scenarios providing the global position of the robot. However, the travelling speed of the robot was essentially defined before the computation of the trajectory, which in practice is an uncertain variable particularly for the terrain robots due to the wheel slippage level.

Additionally, an immense body of previous research has assumed the mobile robots being ideally capable of converting the entire delivered torque at the wheels into motion, alternatively described as slippage-free pure rotation of the wheels [24]. However, the attributed nonholonomic constraints are insufficient to describe the dynamics of deformable terrain based-wheeled robot motioning essentially due to the elastic-plastic behavior of the terrain under the shear-compression loads. It is comprehensively understood that wheel skidding and slipping effects remains a huge effect on the controllability and maneuverability of mobile robots owing to the wheel slippage on terrain. However, there has not been sufficiently dedicated to the terrain-based robots running on deformable terrains where the directional wheel slippage is of primary importance. Moreover, the deformable terrains produce massive fluctuations in the correcting force magnitude due to the wheel-soil adhesive forces. Besides the directional adjusting forces, the lateral stability of the robot is provided by the shear forces developed at the contact patch. The lateral force, however, can be insufficient to counterbalance the centrifugal force, particularly under high-speed or at sharp corners generating even larger side-slip

of the wheel. Thus, it is essential to comprehend the full dynamics of the moving robot on deformable terrain by employing the Terramechanics laws and the interactions between these complex systems.

In light of the reviewed literature, it is inferred that the machine learning based strategies, such as RL, have demonstrated superior performance with regard to the learning the dynamics of nonlinear and complex robotic systems and also for the control of wheeled robots for path-tracking and collision avoidance tasks. However, there are certain aspects related to RL in terms of the convergence and optimization procedure are still regarded as the challenging premises. This paper mainly contributes to the available literature by i) incorporating the Terramechanics laws for the slip-velocity estimations related to the dynamics of a nonholonomic terrain-based robot, and ii) employing a proposed Single-Time Velocity Estimator principle integrated by a chaotic metaheuristics-based Q-learning algorithm for the control of the robot to avoid collision with the dynamic obstacles in order to reach the final target location.

II. PROBLEM FORMULATION
A. TERRAMECHANICS MODEL
The principles related to terrain mechanics are employed to formulate the dynamics of the robot under the effect of the developed torque and force at the contact-patch. The principle includes the generation and propagation of the normal and shear stresses at the contact-patch that finally form the driving forces and moments. The magnitude of shear stress τ_x generated at the soil-wheel contact patch is described based on the following principle [25]:

$$\tau_x = \tau_{max}\left(1 - e^{-\frac{j_x}{k_x}}\right) \tag{1}$$

where j_x defines the shear deformation, k_x represents the longitudinally oriented shear deformation modulus, τ_{max} denotes the limiting shear stress based on a coupling term related to the normal stress σ_n as follows [25]:

$$\tau_{max} = \left(C + \sigma_n \tan \varphi^*\right) \tag{2}$$

where C and φ^* represent the cohesion and shear resistance angle characteristic soil. Consequently, soil shear displacement j_x can be calculated based on the time-integration of the soil profile shear velocity due to the interaction with the rotating wheel [26]:

$$j_x(\theta) = \int_{-\theta_r}^{\theta_e} R\left[1 - (1 - S)\cos\theta\right]d\theta \tag{3}$$

where R and S are the wheel radius and longitudinal slippage parameters, respectively. Additionally, θ denotes the angular position of the wheel segment that launches the rotation in the counterclockwise direction with respect to the wheel center, and θ_e represents the frontal contact patch angle (Fig. 1). The relationship presented in (3) also defines the shear deformation j_x as a function of the wheel slip magnitude S, in a manner that the soil shear displacement grows with the slip value
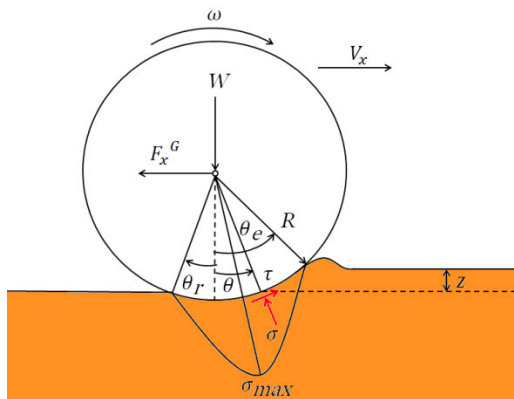
FIGURE 1. Interaction between driven rigid wheel of robot and deformable terrain.

increment. Similarly, the soil shear displacement in the lateral direction, j_y, is defined by employing a related principle in terms of the time-integration of the soil profile shear velocity projection based on the side-slip angle value:

$$j_y(\theta) = \int_0^t V_y dt = \int_{-\theta_r}^{\theta_e} V_x \tan\alpha \, d\theta \quad (4)$$

where V_x and V_y represent the directional speeds of the rotating wheel and α denotes the yaw angle according to

$$\alpha = arctan\left(\frac{V_y}{V_x}\right) \quad (5)$$

Additionally, the wheel slip value under the acceleration and braking modes of motion are expressed as follows:

$$S = \begin{cases} 1 - \dfrac{V_x}{R\omega} & R\omega > V_x \; (acceleration) \\ \dfrac{R\omega}{V_x} - 1 & V_x > R\omega \; (deceleration) \end{cases} \quad (6)$$

where ω represents the rate of wheel angular displacement. By incorporating the relationships (1), (2) and (4), the lateral shear stress term τ_{ycp} for the entire contact area (A) can be described as:

$$\tau_{ycp} = \left(C + \sigma_n \tan\varphi^*\right)\left(1 - e^{-\frac{j_y}{k_y}}\right) \quad (7)$$

where k_y denotes the soil lateral shear deformation modulus to obtain the generated lateral shear force by the time-integration of the shear stress in the contact area assuming the contact width remains constantly the same as the wheel width b. It can be also appreciated based on (7) that the shear stress expands across the contact length with the increase of the soil lateral shear displacement. Accordingly, the amount of the entire shear deformation parameter is expressed as:

$$j = \sqrt{j_x^2 + j_y^2} \quad (8)$$

The magnitude of perpendicular force applied to the terrain from the rotating wheel brings about a certain soil sinkage. The occurred soil sinkage can be formulated on account of the pressure-sinkage relationship that accounts for the soil

bearing capacity. The radially oriented pressures at the contact patch are employed to derive the acting moments and forces on the driven rigid wheel. Bekke's technique assumes that wheel is rigid enough to deform and sinks into the soil profile [25]. Based on this principle, the forces applied to the wheel during the time-integral related to the soil-wheel stress components at the contact patch. Accordingly, the normal stress is obtained based on the pressure-sinkage relationship [27].

$$\sigma_n = \left(\frac{k_c}{b} + k_\varphi\right) z^n \quad (9)$$

where z, n and b denote the wheel sinkage into the soil, exponent factor, and the width of the wheel, respectively. For small sinkage ratios, the contact length is considered in (9), and, k_c and k_φ are soil coefficients [25]. However, there are two substantial limiting factors, related to *i*) insufficient capacity of the unified equation to consider the various plate shapes employed in the sinkage tests, and *ii*) the absence of varying soil bulk density due to soil sinkage/compaction [26]. Instead, a modified form of the relationship, Bekker-Reece equation, is presented based on σ_n

$$\sigma_n(\theta) = \left(Ck_c' + b\gamma_s k_\varphi'\right)\left(\frac{z}{b}\right)^n \quad (10)$$

where k_c', k_φ' represents soil texture cohesion and friction constants based on the Bekker-Reece relationship [25]. Based on the reviewed literature associated with various soil textures, the exponent is generally ranged between 0.8 and 1.2 [25]. Soil cohesion constant is derived using either uni-axial or tri-axial compression tests [28]. The normal stress developed in the front (σ_{nf}) and rear (σ_{nr}) sections in the wheel-soil interface can be considered asymmetric (Fig.1), and can be formulated as follows [26]:

$$\sigma_n(\theta) = \begin{cases} \sigma_{nf}(\theta) & 0 < \theta < \theta_e \\ \sigma_{nr}(\theta) & \theta_r < \theta < 0 \end{cases} \quad (11)$$

where

$$\sigma_{nf}(\theta) = \left(Ck_c' + b\gamma_s k_\varphi'\right)\left(\frac{R(\cos\theta - \cos\theta_e)}{b}\right)^n \quad (12)$$

$$\sigma_{nr}(\theta) = \left(Ck_c' + b\gamma_s k_\varphi'\right) \\ \times \left(\frac{R}{b}\left(\cos\theta_e - \left(\frac{\theta - \theta_r}{\theta_N - \theta_r}\right)(\theta_e - \theta_N)\right)\right)^n \quad (13)$$

where θ_N denotes the angle for the maximum stress point based on the contact patch center value. The longitudinal force generated due to the soil compaction/thrust accounting for the external force applied the robot is computed as:

$$F_x^G = Rb\left(\int_{-\theta_r}^{\theta_e} \sigma_n(\theta)\sin\theta d\theta - \int_{-\theta_r}^{\theta_e} \tau(\theta)\cos\theta d\theta\right) \quad (14)$$

where τ and σ_n represent the shear stress at the surface of the wheel-soil and the normal stress component, respectively. The above relationships are functional for the rigid-wheel based mobile robots where the wheel radius remains unchanged but the stress field is regarded with
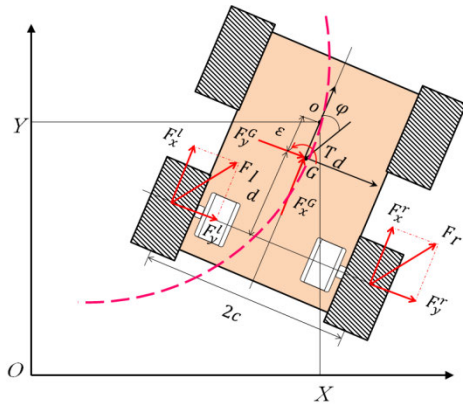
FIGURE 2. Schematic illustration of the wheeled nonholonomic robot (body-fixed coordinate system, oxy) including two independent driving wheels to follow the desired trajectory in the global coordinate system OXY subjected to the wheel slippage and external disturbances.

nonuniform distribution. It is also noteworthy that the first and second components in equations (14) represent the shear thrust and soil compaction resistance, respectively.

B. PROBLEM FORMULATION FOR ROBOT WHEEL WITH SLIPPAGE AND EXTERNAL DISTURBANCE

The governing equations of motion related to a nonholonomic wheeled mobile robot are developed by employing a body-fixed coordinate system. In this paper, the rear wheels are employed as driving wheels where the front wheels are free-rolling wheels without any slippage. The free body diagram of the wheeled robot in the yaw-plane of motion is shown in Fig. 2, exhibiting the independently actuated rear wheels. The optimal torque for the rear wheels to carry out the desired path following on a deformable soil is developed utilizing the electric motors. The kinematic equations are obtained based on the constraints of the velocity components. For a given value of the right and left wheel rotational velocities, the longitudinal and lateral speeds and the yaw rate of the robot are formulated as:

$$\omega_l = \frac{(V_{xl} + S_l)}{R}; \quad \omega_r = \frac{(V_{xr} + S_r)}{R} \quad (15)$$

$$v_x = \frac{(V_{xl} + V_{xr})}{2}; \quad v_y = \frac{d(V_{xl} - V_{xr})}{2c} + S_k \quad (16)$$

$$r_b = \frac{(V_{xl} - V_{xr})}{2c} \quad (17)$$

where ω_l and ω_r are the rotational velocities of the left and right side wheels, v_x and v_y are the body-fixed longitudinal and lateral velocities of the robot at its center gravity (CG) (G). Additionally, r_b represents the yaw rate, V_{xl} and V_{xr} denote the longitudinal velocities of the side wheels. Furthermore, S_k indicates the wheel skidding, S_r and S_l represent the right and left side wheel slip values, c is half-track width, and d is longitudinal distance between the rear wheels to CG. The wheel slippage includes the major velocity components: S_r and S_l, and S_k for the braking term. The path-tracking trajectory of the wheeled robot and the heading angle can be

expressed as follows.

$$r_b = \dot{\varphi} \quad (18)$$

$$\dot{Y} = v_x \sin\varphi - v_y^o \cos\varphi = v_x \sin\varphi - (v_y + \varepsilon r_b) \cos\varphi \quad (19)$$

$$\dot{X} = v_x \cos\varphi + v_y^o \sin\varphi = v_x \cos\varphi + (v_y + \varepsilon r_b) \cos\varphi \quad (20)$$

where X and Y represent the global coordinates, φ, ε and v_y^o denote the yaw angle, longitudinal distance between the robot center CG (G) and the tracking point O, and the lateral velocity at point O, respectively. Based on Newton's second law, the governing equations of motion for the robot are derived considering 5 degrees-of-freedom (DOF) can be formulated as

$$\dot{v}_y = \frac{1}{m}\left(F_y^r + F_y^l + F_y^G\right) - v_x r_b \quad (21)$$

$$\dot{v}_x = \frac{1}{m}\left(F_x^r + F_x^l + F_x^G\right) + v_y r_b \quad (22)$$

$$\dot{r}_b = \frac{1}{I_z}\left\{\left(F_x^l - F_x^r\right)c - \left(F_y^l + F_y^r\right)d - T_d\right\} \quad (23)$$

$$\dot{\omega}_l = \frac{1}{I_w}\sum T_w^l = \frac{1}{I_w}\left(\eta T_l - RF_x^l\right) \quad (24)$$

$$\dot{\omega}_r = \frac{1}{I_w}\sum T_w^r = \frac{1}{I_w}\left(\eta T_r - RF_x^r\right) \quad (25)$$

where $F_y^r, F_y^l, F_x^r, F_x^l$ represent the forces exerted on the right and left driving wheels in the lateral and longitudinal directions, respectively. Additionally, F_x^G, F_y^G denote the external forces due to the deformable soil characteristics, and T_d acts as the external moment to the robot frame ($F_y^G = \tau_{ycp}A$, $T_d = F_y^G d + F_x^G c$). Furthermore, F_x^r, F_x^l depend on of the applied input torque to the right and left wheels, respectively. Moreover, the lateral force components F_y^r, F_y^l are linked to the longitudinal components via the sideslip angle of the whee αl. Additionally, m, η, I_z and I_w characterize the total robot mass, gear ratio related to the motor drives, mass moment of inertia in the yaw plane, and the equivalent mass moment of inertia associated with the wheel and the driving motor, respectively. Finally, T_l and T_r denote the applied input torques to the left and rights wheels, respectively. Rearranging (23)-(27) taking into account the kinematic formulations (15)-(22), the state-space representation of the model is obtained as:

$$\dot{x} = \mathbf{F}(\mathbf{x}) + \mathbf{H}(\mathbf{u}) + \mathbf{D} \quad x \in R^5, \ u \in R^2 \quad (26)$$

where $\mathbf{x} = [r_b, v_x, \varphi, Y, X]^T$ and $\mathbf{u} = \left[T_1^*, T_2^*\right]^T$ represent the states and the inputs to the system and additionally:

$$\mathbf{F} = \begin{bmatrix} \dfrac{-mdv_x r_b R^2}{R^2\left(I_z + md^2\right) + 2c^2 I_w} \\ \dfrac{mdr_b^2 R^2}{2I_w + mR^2} \\ r_b \\ v_x \sin\varphi + (dr_b + \varepsilon r_b)\cos\varphi \\ v_x \cos\varphi - (dr_b + \varepsilon r_b)\sin\varphi \end{bmatrix},$$

$$H = \begin{bmatrix} 0 & \dfrac{\eta cR}{R^2\left(I_z + md^2\right) + 2c^2 I_w} \\ \dfrac{\eta cR}{2I_w + mR^2} & 0 \\ 0 & 0 \\ 0 & 0 \\ 0 & 0 \end{bmatrix} \quad \text{and}$$

$$D = \begin{bmatrix} \dfrac{cI_w\left(\dot{v}_{xr} - \dot{v}_{xl}\right) + \left(dF_y^G - T_d - md\dot{S}_k\right)R^2}{R^2\left(I_z + md^2\right) + 2c^2 I_w} \\ \dfrac{\left(F_y^G + mr_b S_k\right)R^2 - I_w\left(\dot{v}_{xr} - \dot{v}_{xl}\right)}{2I_w + mR^2} \\ 0 \\ S_k \cos\varphi \\ -S_k \sin\varphi \end{bmatrix} \quad (27)$$

where $T_1^* = T_l + T_r$ and $T_2^* = T_l - T_r$, and F, H, and D represent the system function, control input and external disturbance, respectively. The tracking point O does not necessarily align with the robot center of mass G. Accordingly, any external forces at the tracking point need to be translated to point G in the form of the equivalent forces and moment.

III. DESIGN OF COLLISION-AVOIDING PATH-PLANNER
A. MULTI-OBJECTIVE-BASED COST FUNCTION
The collision avoidance problem related to the nonholonomic robot can be described in the form of a constrained optimization problem. Such an optimization problem can be formulated to minimize the start-to-target trajectory path while avoiding to collide the moving/stationary obstacles over a given time horizon. Accordingly, a cost function can be described as:

$$J = \min_{T_1^*, T_2^*} \left[w_1 J_o + w_2 J_t \right] \quad (28)$$

where

$$\begin{cases} J_o = \left\{ \dfrac{1}{2} \sum_{k=0}^{T_f - 1} \left[\begin{matrix} \left(\dot{X}_k - \dot{X}_k^{ob}\right)^T Q_1 \left(\dot{X}_k - \dot{X}_k^{ob}\right) \\ + \left(\dot{Y}_k - \dot{Y}_k^{ob}\right)^T Q_2 \left(\dot{Y}_k - \dot{Y}_k^{ob}\right) \end{matrix} \right], \Xi \right\} \\ J_t = \dfrac{1}{2} \int_0^{T_f} \left[\begin{matrix} \left(\dot{X} - \dot{X}_t\right) Q_3 \left(\dot{X} - \dot{X}_t\right)^T \\ + \left(\dot{Y} - \dot{Y}_t\right) Q_3 \left(\dot{Y} - \dot{Y}_t\right)^T \end{matrix} \right] dt \end{cases}$$

$$(29)$$

where, and $[0, T_f]$ represents the optimization horizon. Moreover, X_t and Y_t are the global positions for the target point, X_k^{ob} and Y_k^{ob} are the obstacle instantaneous positions, Ξ serves as the factor related to the collision risk parameter which regulates the obstacle distance at which, the robot should be trained to avoid to decrease the distance, w_1 and w_2 are the adjusting weights for the cost function, and Q_i $i = 1, 2, 3, 4$ acts as the adjusting matrix weight chosen arbitrarily to converge the robot towards the objective in different directions. The constraints on the initial and final values of the problem are stated as follows:

$$X(0) = Y(0) = 0, \quad X\left(T_f\right) = Y\left(T_f\right) = 26 \quad (30)$$

Describing the robot position in the global coordination at the start of the problem and the target where the robot is intended to reach without colliding with the obstacles in an optimal manner at the end of simulation. The instantaneous physical limits of the terrain robot to the states and the control inputs according to (26) and (27) and by employing the proposed algorithm can be proposed as:

$$0 \leq X(t), Y(t) \leq X_{max}, Y_{max} \quad t \subset [0, T_f]$$
$$T_{min}^* \leq T_i^* \leq T_{max}^* \quad i = 1, 2$$
$$\varphi_{min} \leq \varphi(t) \leq \varphi_{max} \quad (31)$$

where the subscripts, min and max, are suggestive of the minimum and maximum thresholds, respectively. In this paper, the nonholonomic terrain robot is controlled for obstacle avoidance and path-planning based on the above optimization objective and constraints by employing a chaotic metaheuristics method and RL-algorithm.

B. METAHEURISTICS-BASED TARGET EXPLANATION
Kennedy and Eberhart [29] first proposed the particle swarm optimization (PSO) algorithm, which has exhibited an extensive applicability within various optimization problems [30]–[32]. However, the standard method in [29] comprises various setbacks related to the premature convergence for multimodal problems [33]. Therefore, the modified versions of the standard PSO in terms of inertia parameter or hybridized optimization algorithms address the convergence and computational demand concerns. In PSO algorithm, the search space is filled with the swarm of particles through a zig-zag-type pattern including two main components concerned with the deterministic and stochastic characteristics [33]. The described components are essential for the particles to slightly shift the location to the current global best $\tilde{x}g_i$, and slightly move towards their own local best $\tilde{x}p_i$ regarded as deterministic movement (Figure 4). Simultaneously, the particles show a random transition during the updates which is known as the stochastic component.

The velocity of a particle can be updated at any incremental time step based on position vector $\tilde{x}$ and velocit v_i:

$$v_i^{t+1} = v_i^t + \alpha r_1 \left(\tilde{x}p_i - \tilde{x}_i^t\right) + \beta r_2 \left(\tilde{x}g_i - \tilde{x}_i^t\right) \quad (32)$$

where $\tilde{x}_i^t$ and v_i^t represent the components of the particle i at time t in terms of position and velocity, respectively. Furthermore, the coefficients r_1 and r_2 are associated with random values distributed uniformly between (0,1) while α and β are the corresponding learning parameters commonly fixed around 2 [33]. Consequently, the updated position vector of an individual particle at the next time step is computed as based on Δt as the step size:

$$\tilde{x}_i^{t+1} = \tilde{x}_i^t + v_i^{t+1} \Delta t \quad (33)$$

However, the premature and sluggish convergence of the PSO algorithm can be modified by incorporating an inertia function term such as $\varphi(t)$ in (32):

$$v_i^{t+1} = \varphi(t) v_i^t + \alpha r_1 \left(\tilde{x}p_i - \tilde{x}_i^t\right) + \beta r_2 \left(\tilde{x}g_i - \tilde{x}_i^t\right) \quad (34)$$
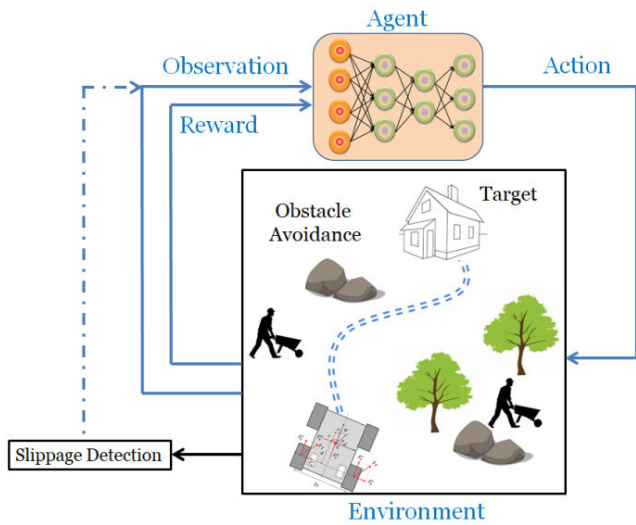
FIGURE 3. Schematic presentation of the nonholonomic terrain robot training for obstacle avoidance and path-planning based on RL-algorithm.
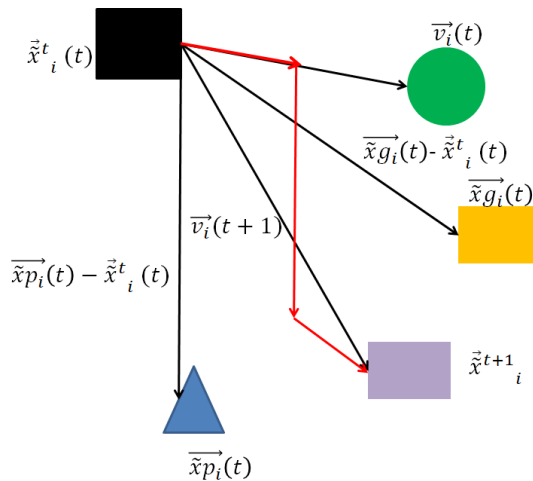

FIGURE 4. Illustration of particle chaotic motions including the position and velocity components.

The inertia function $\varphi(t)$ can be assigned any magnitude ranging between 0.5 and 0.9 [34]. The inertia term is mainly employed to enhance a stabilizer for the particles during the evolution and transitions to improve the convergence in the optimization problem. Therefore, it is essential to begin the problem optimization by setting the inertia function at a relatively large constant value and then vary the parameter during the iterations (epochs). The classical PSO algorithm utilizes the position of the present global best $\tilde{x}g_i$, and slightly that of particle local best $\tilde{x}p_i$. A primary purpose for utilizing the local best is essentially to improve the heterogeneity in the solution; while such an end can be achieved within by introducing some randomness and chaotic motion of the particles. A simplified model of accelerated convergence with the application of solely a global best was proposed by Yang [35], where the velocity vector was updated as:

$$v_i^{t+1} = v_i^t + \alpha r(t) + \beta r_2 \left(\tilde{x}g_i - \tilde{x}_i^t\right) \quad (35)$$

where $r(t)$ represents the vector of randomly selected values distributed uniformly between (0,1). Therefore, the position of each particle is updated, as follows

$$\tilde{x}_i^{t+1} = (1 - \beta)\tilde{x}_i^t + \beta\tilde{x}g_i + \alpha r(t) \quad (36)$$

This approach yields greater convergence performance because updating of the position is implemented independent of the velocity components, as seen in (36). This optimization problem based on the chaotic transition of the particles is employed for the problem (28) and (29) subject to constraints (30) and (31).

C. SINGLE-TIME VELOCITY ESTIMATOR

The velocity of the robot can be predicted as a Markov chain, where the transition probability of the velocity is formulated using the maximum likelihood predictor and the nearest neighbor principle:

$$p_{\Phi\kappa}(k) = P\left(v_i^{k+1} = \kappa | v_i^k = \Phi\right)$$

$$= \left(\sum\nolimits_{\kappa=1}^{\rho} S_{\Phi\kappa}\right)^{-1} S_{\Phi\kappa} \quad i = x, y \quad (37)$$

where $p_{\Phi\kappa}(k)$ represents the one-step transition probability as the robot velocity transfers from Φ at time k to κ at next time $k + 1$, $\sum_{\kappa=1}^{\rho} S_{\Phi\kappa}$ is the transition number from Φ to κ, and $S_{\Phi\kappa}$ describes the total transition number initiated from k. Furthermore, the transition probability matrix Π is filled with element $p_{\Phi\kappa}$. The probability vector related to the one-step-ahead of the robot in the plane of motion, $\{v_i, i = x, y\}$, can arbitrarily adopt one of finite values v_j.

$$\Pi = p_{\Phi\kappa}(k+1)^T \left((p_{\Phi\kappa}(k))^T\right)^{-1} \quad (38)$$

and,

$$\Pi^k = p_{\Phi\kappa}(+k) / p_{\Phi\kappa}(k+1) \quad (39)$$

Based on the one-step transition probability matrix, the future driving cycle is predicted as follows:

$$\left(v_i^{k+1}\right)_p = \sum\nolimits_{\kappa=1}^{\rho} S_{\Phi\kappa}.v_i^k \quad i = x, y \quad (40)$$

where $\left(v_i^{k+1}\right)_p$ is robot predicted velocity in the longitudinal and lateral directions based on the prediction value, while the singe-time prediction is achieved by repeating the above process during the entire running time.

D. REINFORCEMENT LEARNING ALGORITHM

The standardized reinforcement learning (RL) models are typically described in terms of an agent that interacts with the environment by employing the action and perception system. During any individual interplay for the action-perception, the agent takes input i as the sign of the present state s of the environment. Subsequently, the agent determines an action a to define the output. Subsequently, the action alternates the environment state and the magnitude related to the associated state transition is taken as the agent by employing a proper

reinforcement signal r. In this system, B is the representative of the agent behavior which determines the corresponding actions in order to enhance the provisional total magnitude related to r, in a reciprocating manner. In such a model representation, the discrete set of environment states denoted by S, as well as a set of discrete agent actions A. Herein, the problem of delayed reinforcement, delayed reward based on a Markov Decision Process (MDP) is employed. Additionally, the reward function $R(R : S \times A \rightarrow \Re)$ and a state transition function T are incorporated ($T : S \times A \rightarrow \Pi(S)$). $\Pi(S)$ is a probability distribution over the set S. The transition function $T(s, s', a)$ is further described by the probability of performing a transition from state s to state s' due to the action a.

In this paper, the infinite horizon discounted model is employed by considering the longer-term reward related to the agent into consideration while the prospective future rewards are topologically discounted based on the discount factor in the range between 0 and 1 ($0 \leq \chi < 1$) such as $E\left(\sum_{t=0}^{\infty} \chi^t r_t\right)$.

The optimal value associated with a state is defined as the average of infinite discounted rewards obtained by an agent to reach the optimality:

$$V^*(s) = \max_\pi E\left(\sum_{t=0}^{\infty} \chi^t r_t\right) \quad (41)$$

Owing to the uniqueness of the optimality function, the solution to the simultaneous equations is defined as a recursion expression [37]:

$$V^*(s) = \max_a \left(R(s, a) + \chi \sum_{s' \in S} T(s, s', a) + V^*(s')\right) \quad \forall s \in S \quad (42)$$

where $V^*(s)$ is the amount of s associated with the initial optimal action. The above statement indicates that the amount of the state is the total sum of the expected instantaneous reward and discounted value of the future state values based on the current action. Based on the optimality policy the desired value function is described as [37]:

$$\pi^*(s) = \underset{a}{\mathrm{argmax}} \left(R(s, a) + \chi \sum_{s' \in S} T(s, s', a) + V^*(s')\right) \quad \forall s \in S \quad (43)$$

Furthermore, the action-value function $Q(s, a)$ is formulated as follows:

$$Q(s, a) = R(s, a) + \chi \sum_{s' \in S} T(s, s', a)Q(s', a') \quad (44)$$

Accordingly, the corresponding optimal solution $Q^*(s, a)$ can be described based on the action-value function

$$Q^*(s, a) = R(s, a) + \chi \sum_{s' \in S} T(s, s', a)Q^*(s', a') \quad (45)$$

where $Q^*(s, a)$ is the expected discounted reinforcement related to the a in state s in a continuous manner. The Q-learning algorithm defines the update related to the Q value based on the delayed parameter Θ ($\Theta \in [0, 1]$) as follows:

$$Q(s, a) := Q(s, a) + \Theta\left(\chi \max_{a'} Q(s', a') - Q(s, a) + r\right) \quad (46)$$

The above adjustment is employed to perform the RL-based predictive decision-making to avoid the obstacle collision by contribution of the time-scale velocity estimator.

IV. RESULTS AND DISCUSSION

The optimal path between the start and target position considering the obstacle avoidance of the nonholonomic terrain robots in the presence of unstructured skidding and slipping is planned by the proposed algorithm during the simulation runs. The obtained results by the proposed chaotic metaheuristic-based Q-learning (RL) integrated by the STV estimator are compared in terms of the root mean square of errors (RMSE) with the adaptive neural network (NN) and multi-agent Lyapunov based control algorithms [24], [36] where the Terramechanics aspects related to the terrain robots are excluded.
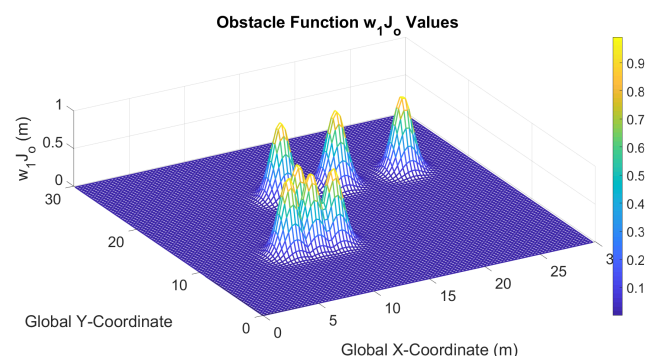

FIGURE 5. Obstacle function and the collision risk propagation in the plane of robot motion.

Figure 5 represents the obstacle function values based on the one-step transition probability in the global surface of motion. Although the location of the stationary/moving obstacles can overrule the optimal path for the robot, the propagation of the risk for the robot to collide these obstacles as a component of the total cost function can be appreciated in Fig. 5, where the collision risk ramps up to a maximum at the center. Additionally, the nucleus growth related to the collision risk is decreased at the further distances.

The combined obstacle collision risk with those of start-target localization in the plane of motion is presented in Figure 6, where the location $X = 0, Y = 0$ defines the starting point and $X = 26, Y = 26$ represents the target position.

The contour plot for the integrated obstacle collision risk function and that of the start to target positions is also presented in Figure 6, where the robot can realize the approaching obstacles (with a total number of 7), and accordingly find the optimal path based on the proposed algorithm. It is noteworthy that the optimal values related to the robot heading angle, yaw rate, and position described in (26)-(27), are obtained based on the average of infinite discounted rewards assigned an agent to reach the optimality subject to (28), (30) and (31) by employing the chaotic-metaheuristics based Q-Learning (41)-(44).
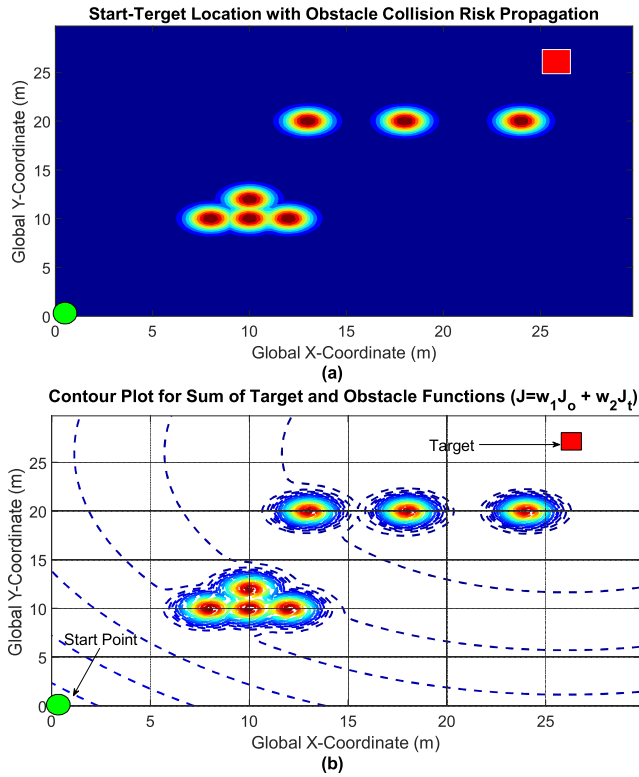
Start-Target Location with Obstacle Collision Risk Propagation

(a)

Contour Plot for Sum of Target and Obstacle Functions ($J=w_1 J_o + w_2 J_t$)

(b)

FIGURE 6. a) Start-Target location with obstacle collision risk propagation; b) contour plot for sum of target and obstacle functions.

Robot Obstacle-Avoidance Trajectory based on Markov Decision Making and STV-Estimator
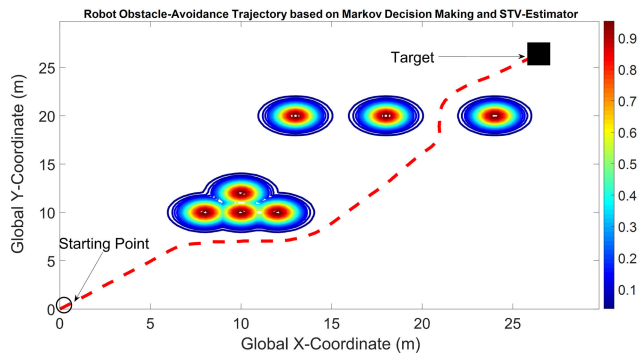
FIGURE 7. Optimal path for the nonholonomic terrain robot subject to unstructured uncertainties from the starting point to the target position based on obstacle avoidance strategy by employing the proposed RL-Algorithm.

The constrained control inputs for the terrain robot are plotted in Figure 7, subject to the deformable terrain induced skid/slip magnitudes formulated in (6) and based on the single-time velocity estimation described in Section 3.3. The control inputs T_1^* and T_2^* that alter the dynamics of the nonholonomic robot according to (26)-(27), are subject to the imposed slip/skid distributions at ± 0.25 occurring at t = 5 s and t = 15 s (Fig. 7). It can be realized that the one-step transition probability related to the proposed RL-algorithm contributes to the rapid realization of the slip/skid effect and to compensate the torque to overcome the effect of the unstructured uncertainties immediately. The individual right-/left-wheel torque are reliably constrained
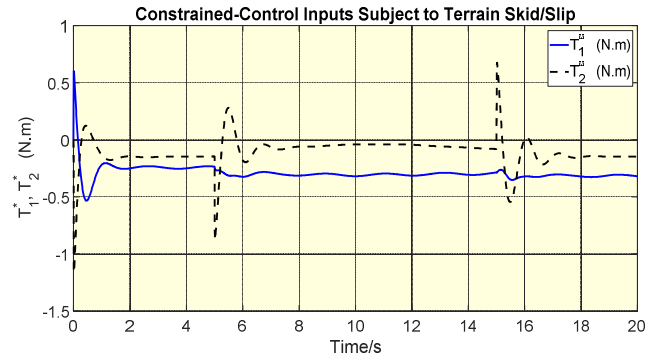
Constrained-Control Inputs Subject to Terrain Skid/Slip

FIGURE 8. Constrained-control inputs related to the proposed chaotic optimization optimally based RL-algorithm system for the right-and left-wheels to run the start-target points.
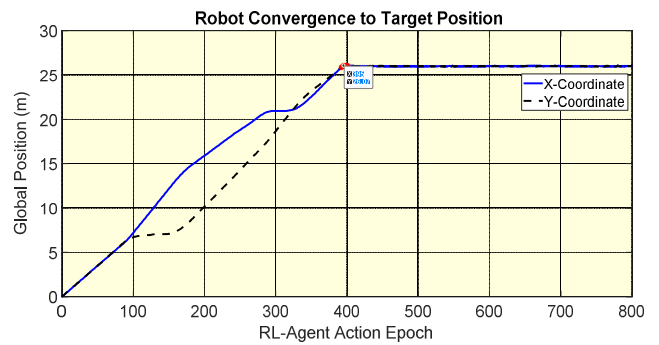
Robot Convergence to Target Position

FIGURE 9. Bidirectional convergence of the robot to the global position based on the action of RL-agents by employing the metaheuristics optimization and STV estimator.

within the minimum-maximum range between $[-1.5, 1.5]$ N.m. It can be seen that the proposed chaotic optimization based RL-algorithm system holds the capacity for the rapid stabilization of the robot.

The bidirectional convergence of the robot to the global position of the target is illustrated in Figure 9 with respect to the epochs of the RL agents with the environment based on the reward policy toward the minimization of the cost function presented in (28) and (29). It can be appreciated that the proposed system generated the rapid learning such that after only 386 iterations (epochs), the system fully converges to the optimal global target point and remains stable for the rest of the simulation time in the prescribed location at $X = 26\ m, Y = 26\ m$. Figure 10 also describes the scenario at which one of the moving obstacles is separated from the nucleus point and shifts the center of the position toward $X = 8\ m, Y = 5\ m$. In this scenario, the robot is able to re-plan the optimal path in terms of the shortest and safest one by avoiding to collide to any obstacle and in order to reach the target point through an entirely different route. The Q-learning based optimized RL-algorithm running based on the velocity estimator is trained sufficiently to perform the maneuvers about the obstacles and reorganize the preplanned path based on the relocation of the environment objects.

It is also known that the adjusting factor χ plays a substantial role in the performance of the robot byfinding the
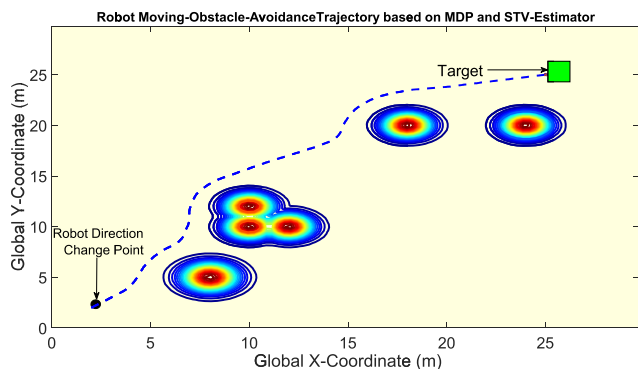
FIGURE 10. Reorganization of the optimal route for the robot based on the moving obstacle in order to avoid the collision by the MDP RL-algorithm and STV-estimator approach.
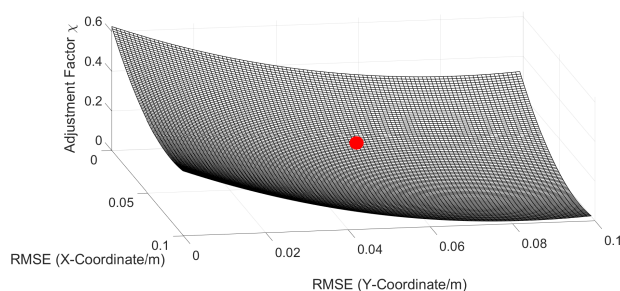

FIGURE 11. Variability of the adjusting factor χ effect related to the proposed RL-algorithm on the RMSE values of the target position errors in the plane of motion.

TABLE 1. Comparative results between the proposed algorithm in this paper, adaptive NN, and formation control algorithms considering the obstacle avoidance strategy and in terms of RMSE.

Control Algorithm	RMSE (Bidirectional Vector Sum)
Adaptive NN [24]	0.12 m
Formation Control [36]	0.17 m
Proposed Algorithm	0.08 m

moving/stationary obstacle avoidance strategy. Furthermore, there are major aspects related to the adoption of the Ter-ramechanics principles to incorporate the influence of wheel sinkage-soil deformation on the response of the mobile robot. The dynamic response of the terrain robot to find optimal path by employing the compensating force/torque magnitude and to sustain a robust and smooth motion was also investigated. Moreover, the developed systematic control-oriented system included a cost function with weighted components concerned with the target-tracking and the obstacle avoidance. A single-time velocity estimator was wrapped up to contribute the finite-state Markov decision process (MDP) in learning the transition probabilities of the problem objectives. On the basis of the simulation results, the optimal solution for the Q-learning in terms of the adjusting factor for the minimized tracking error and obstacle collision risk propagation profiles was obtained at 0.22. In light of the obtained results and the comparisons made, it was observed that the proposed algorithm has the ability to perform the collision avoidance of the nonholonomic robots on deformable terrains accurately and effectively.

optimal value associated with a state as the average of infinite discounted rewards through the agents according to (40). As appreciated from Fig. 11, the optimal value related to the adjusting factor χ based on the RMSE of convergence to the final target position in the plane of motion is achieved at 0.22 while further decrease/increase of the adjusting factor could slightly affect either of the directional positioning errors.

Finally, the results of the proposed chaotic metaheuristics based optimization integrated by the transition-based RL-algorithm compared to [24] and [36] are presented in Table 1. Based on the presented results, it is clear that the proposed algorithm holds the capacity for a generic learning based on the agents' action with the environment when compared to the adaptive NN and formation control in terms of the RMSE of the target position. The improved performance related to the proposed algorithm is also attributed to the estimation of the wheel skid/slip values by incorporation of the Ter-ramechanics principles explained in Section 2.1. Based on the obtained results, it can be concluded that the proposed optimization-based RL algorithm holds the promising capacity for the collision avoidance control of the nonholonomic robots on deformable terrains.

In this paper, a single-time velocity estimator based reinforcement learning (RL) algorithm, integrated with a chaotic metaheuristics optimization technique was employed for the optimal path-planning of the nonholonomic terrain robots. Additionally, the proposed algorithm considers the

REFERENCES

[1] A. Sgorbissa, "Integrated robot planning, path following, and obstacle avoidance in two and three dimensions: Wheeled robots, underwater vehicles, and multicopters," *Int. J. Robot. Res.*, vol. 38, no. 7, pp. 853–876, Jun. 2019.

[2] S. M. H. Rostami, A. K. Sangaiah, J. Wang, and H. J. Kim, "Real-time obstacle avoidance of mobile robots using state-dependent Riccati equation approach," *EURASIP J. Image Video Process.*, vol. 2018, no. 1, p. 79, Dec. 2018.

[3] A. Alomari, W. Phillips, N. Aslam, and F. Comeau, "Swarm intelligence optimization techniques for obstacle-avoidance mobility-assisted localization in wireless sensor networks," *IEEE Access*, vol. 6, pp. 22368–22385, 2018.

[4] F. Y. Narvaez, G. Reina, M. Torres-Torriti, G. Kantor, and F. A. Cheein, "A survey of ranging and imaging techniques for precision agriculture phenotyping," *IEEE/ASME Trans. Mechatronics*, vol. 22, no. 6, pp. 2428–2439, Dec. 2017.

[5] Y. Qin, Z. Wang, C. Xiang, M. Dong, C. Hu, and R. Wang, "A novel global sensitivity analysis on the observation accuracy of the coupled vehicle model," *Vehicle Syst. Dyn.*, vol. 57, no. 10, pp. 1445–1466, 2019.

[6] Y. Qin, J. J. Rath, C. Hu, C. Sentouh, and R. Wang, "Adaptive nonlinear active suspension control based on a robust road classifier with a modified super-twisting algorithm," *Nonlinear Dyn.*, vol. 97, no. 4, pp. 2425–2442, Sep. 2019.

[7] C. Hu, Z. Wang, H. Taghavifar, J. Na, Y. Qin, J. Guo, and C. Wei, "MME-EKF-based path-tracking control of autonomous vehicles considering input saturation," *IEEE Trans. Veh. Technol.*, vol. 68, no. 6, pp. 5246–5259, Jun. 2019.

[8] W. Li and R. Xiong, "Dynamical obstacle avoidance of task-constrained mobile manipulation using model predictive control," *IEEE Access*, vol. 7, pp. 88301–88311, 2019.

[9] D. González, J. Pérez, V. Milanés, and F. Nashashibi, "A review of motion planning techniques for automated vehicles," *IEEE Trans. Intell. Transp. Syst.*, vol. 17, no. 4, pp. 1135–1145, Apr. 2016.

[10] J. Alonso-Mora, P. Beardsley, and R. Siegwart, "Cooperative collision avoidance for nonholonomic robots," *IEEE Trans. Robot.*, vol. 34, no. 2, pp. 404–420, Apr. 2018.

[11] H. Chuan, W. Zhenfeng, and Q. Yechen, "Lane keeping control of autonomous vehicles with prescribed performance considering the rollover prevention and input saturation," *IEEE Trans. Intell. Transp.*, to be published, doi: 10.1109/TITS.2019.2924937.

[12] A. Babinec, F. Duchoň, M. Dekan, Z. Mikulová, and L. Jurišica, "Vector Field Histogram with look-ahead tree extension dependent on time variable environment," *Trans. Inst. Meas. Control*, vol. 40, no. 4, pp. 1250–1264, 2018.

[13] E. J. Molinos, Á. Llamazares, and M. Ocaña, "Dynamic window based approaches for avoiding obstacles in moving," *Robot. Auton. Syst.*, vol. 118, pp. 112–130, Aug. 2019.

[14] N. Uchiyama, T. Hashimoto, S. Sano, and S. Takagi, "Model-reference control approach to obstacle avoidance for a human-operated mobile robot," *IEEE Trans. Ind. Electron.*, vol. 56, no. 10, pp. 3892–3896, Oct. 2009.

[15] S. X. Yang, A. Zhu, G. Yuan, and M. Q.-H. Meng, "A bioinspired neurodynamics-based approach to tracking control of mobile robots," *IEEE Trans. Ind. Electron.*, vol. 59, no. 8, pp. 3211–3220, Aug. 2011.

[16] Z. Peng, G. Wen, A. Rahmani, and Y. Yu, "Leader–follower formation control of nonholonomic mobile robots based on a bioinspired neurodynamic based approach," *Robot. Auto. Syst.*, vol. 61, no. 9, pp. 988–996, Sep. 2013.

[17] H. Kim and B. K. Kim, "Online minimum-energy trajectory planning and control on a straight-line path for three-wheeled omnidirectional mobile robots," *IEEE Trans. Ind. Electron.*, vol. 61, no. 9, pp. 4771–4779, Sep. 2014.

[18] Z. Zhou, C. Du, L. Shu, G. Hancke, J. Niu, and H. Ning, "An energy-balanced heuristic for mobile sink scheduling in hybrid WSNs," *IEEE Trans. Ind. Informat.*, vol. 12, no. 1, pp. 28–40, Feb. 2016.

[19] N. Ganganath, C.-T. Cheng, and C. K. Tse, "A constraint-aware heuristic path planner for finding energy-efficient paths on uneven terrains," *IEEE Trans. Ind. Informat.*, vol. 11, no. 3, pp. 601–611, Jun. 2015.

[20] C. Wu, B. Ju, Y. Wu, X. Lin, N. Xiong, and G. X. Xu Liang, "UAV autonomous target search based on deep reinforcement learning in complex disaster scene," *IEEE Access*, vol. 7, pp. 117227–117245, 2019.

[21] L. Roveda, G. Pallucca, N. Pedrocchi, F. Braghin, and L. M. Tosatti, "Iterative learning procedure with reinforcement for high-accuracy force tracking in robotized tasks," *IEEE Trans. Ind. Informat.*, vol. 14, no. 4, pp. 1753–1763, Apr. 2018.

[22] G. Sartoretti, J. Kerr, Y. Shi, G. Wagner, T. K. S. Kumar, S. Koenig, and H. Choset, "PRIMAL: Pathfinding via reinforcement and imitation multi-Agent learning," *IEEE Robot. Autom. Lett.*, vol. 4, no. 3, pp. 2378–2385, Jul. 2019.

[23] M. Duguleana and G. Mogan, "Neural networks based reinforcement learning for mobile robots obstacle avoidance," *Expert Syst. Appl.*, vol. 62, pp. 104–115, Nov. 2016.

[24] S. J. Yoo, "Adaptive neural tracking and obstacle avoidance of uncertain mobile robots with unknown skidding and slipping," *Inf. Sci.*, vol. 238, pp. 176–189, Jul. 2013.

[25] J. Y. Wong, *Terramechanics and Off-Road Vehicles*. Amsterdam, The Netherlands: Elsevier, 1989.

[26] H. Taghavifar and A. Mardani, *Off-Road Vehicle Dynamics* (Studies in Systems, Decision and Control). Berlin, Germany: Springer, 2017.

[27] M. G. Bekker, *Theory of Land Locomotion*. Ann Arbor, MI, USA: Univ. of Michigan Press, 1956.

[28] N. E. Dowling, *Mechanical Behavior of Materials: Engineering Methods for Deformation, Fracture, and Fatigue*. Upper Saddle River, NJ, USA: Prentice-Hall, 1993.

[29] J. Kennedy and R. Eberhart, "Particle swarm optimization," in *Proc. IEEE Int. Conf. Neural Netw.*, Nov. 1995, pp. 1942–1948.

[30] H. Taghavifar and A. Mardani, "Energy loss optimization of run-off-road wheels applying imperialist competitive algorithm," *Inf. Process. Agricult.*, vol. 1, no. 1, pp. 57–65, Aug. 2014.

[31] H. Pang, F. Liu, and Z. Xu, "Variable universe fuzzy control for vehicle semi-active suspension system with MR damper combining fuzzy neural network and particle swarm optimization," *Neurocomputing*, vol. 306, pp. 130–140, Sep. 2018.

[32] M. Gohari and M. Tahmasebi, "Off-road vehicle seat suspension optimisation, Part II: Comparative study between meta-heuristic optimisation algorithms," *J. Low Freq. Noise, Vib. Act. Control*, vol. 33, no. 4, pp. 443–454, 2014.

[33] A. H. Gandomi, G. J. Yun, X.-S. Yang, and S. Talatahari, "Chaos-enhanced accelerated particle swarm optimization," *Commun. Nonlinear Sci. Numer. Simul.*, vol. 18, no. 2, pp. 327–340, Feb. 2013.

[34] M. Clerc and J. Kennedy, "The particle swarm-explosion, stability, and convergence in a multidimensional complex space," *IEEE Trans. Evol. Comput.*, vol. 6, no. 1, pp. 58–73, Feb. 2002.

[35] X.-S. Yang *Engineering Optimization: An Introduction With Metaheuristic Applications*. Hoboken, NJ, USA: Wiley, 2010.

[36] S. Mastellone, D. M. Stipanović, C. R. Graunke, K. A. Intlekofer, and M. W. Spong, "Formation control and collision avoidance for multi-agent non-holonomic systems: Theory and experiments," *Int. J. Robot. Res.*, vol. 27, no. 1, pp. 107–126, Jan. 2008.

[37] T. Liu, X. Hu, W. Hu, and Y. Zou, "A Heuristic planning reinforcement learning-based energy management for power-split plug-in hybrid electric vehicles," *IEEE Trans. Ind. Informat.*, to be published.

HAMID TAGHAVIFAR (M'18) received the Ph.D. degree in mechanical from Urmia University, Iran, in 2016. He was a Horizon Postdoctoral Fellow with the CONCAVE Research Center, Department of Mechanical, Industrial and Aerospace Engineering, Concordia University, Canada. He is currently an Assistant Professor with the School of Mechanical, Aerospace and Automotive Engineering, Coventry University, U.K. His research interests include vehicle dynamics and control, terramechanics and mechatronics, adaptive and nonlinear controls, artificial intelligence, and optimizations. In the above fields, he has contributed over 45 articles, a book, and two Iranian registered patents. He serves as the Editor-in-Chief for *Journal of Advances in Vehicle Engineering* and an Editor for *International Journal of Vehicle Systems Modeling and Testing* and *International Journal of Vehicle Information and Communication Systems*.

BIN XU received the B.Sc. and Ph.D. degrees in mechanical engineering from the Beijing Institute of Technology, China, in 2005 and 2013, respectively. He is currently an Associate Professor with the Vehicle Research Center, Beijing Institute of Technology. His research interests include aerial and ground vehicle, and its dynamic control.

LEYLA TAGHAVIFAR received the B.Sc. and M.Sc. degrees in electrical engineering from Tabriz University and IAU, Tehran, Iran, in 2009 and 2013, respectively. Her research interests include signal processing and synchronization, telecommunications, cellular networks, and artificial intelligence.

YECHEN QIN (S'14–M'17) received the B.Sc. and Ph.D. degrees in mechanical engineering from the Beijing Institute of Technology, China, in 2010 and 2016, respectively. From 2013 to 2014, he was a Visiting Ph.D. Student with Texas A&M University, USA. He was a Postdoctoral Research Fellow and a Visiting Scholar with the Beijing Institute of Technology and University of Waterloo, respectively. He is currently an Associate Professor with the Beijing Institute of Technology. His research interests include vehicle dynamics control and road estimation.